



Search for new apatite-like phases for lead utilization based on crystal structure and thermal expansion

EVGENY N. BULANOV*, ANASTASYYA A. VASILEVA, OXANA N. GOLITSYNA,
ALYONA G. SHVAREVA and ALEXANDER V. KNYAZEV

Lobachevsky University, 23 Gagarin ave, Nizhny Novgorod 603022, Russia

(Received 24 July, revised 31 July, accepted 18 September 2023)

Abstract: Apatites, being one of the most numerous mineral-like families of compounds, are considered as a matrix for binding lead ions, which is dangerous for the biosphere. The crystal-chemical (composition, structure) and thermophysical aspects (thermal expansion) are considered as the basis for analysing the properties of this kind of material. It is suggested that substances of the composition $Pb_5(A^{IV}O_4)_2(B^{VI}O_4)$, $Pb_5(A^{IV}O_4)(C^V O_4)_2$ can be a perspective form of lead binding materials based on compounds with the structure of apatite (A^{IV} = Si, Ge; B^{VI} = S, Cr; C^V = P). Such compounds, as it was shown by DTA and HTXRD experiments, are distinguished by the absence of polymorphism and the abnormal ordering of structure. Also, they have relatively low values of thermophysical indicators (the rate of change of linear thermal expansion coefficients is $0.02\text{--}0.03 \times 10^6 \text{ K}^{-1}$; values of the volume thermal expansion coefficients are $40\text{--}70 \times 10^6 \text{ K}^{-1}$). Compounds $Pb_5(SiO_4)(PO_4)_2$ ($a = 9.78782(16)$ Å, $c = 7.31084(16)$ Å, $V = 606.555(23)$ Å 3 , $R\text{-bragg} = 4.694\%$) and $Pb_5(GeO_4)(PO_4)_2$ ($a = 9.87697(12)$ Å, $c = 7.33136(11)$ Å, $V = 619.388(17)$ Å 3 , $R\text{-bragg} = 1.730\%$) were obtained, identified and crystallographically characterised for the first time.

Keywords: lead; apatite; IR spectroscopy; Rietveld analysis; *in situ* HTXRD; thermal expansion.

INTRODUCTION

Environmental pollution is one of the global environmental problems of mankind. Soil pollution is particularly dangerous, since 90–95% of food products account for soil resources, from where 70–90% of toxins (including heavy metals) enter the body. It causes a chain reaction – the filtering capacity of the soil decreases, organic matter reserves and biodiversity decrease too; toxicants can enter groundwater from contaminated soil; then they accumulate in plant tissues and are transmitted to pasture animals, birds and finally to humans.¹

* Corresponding author. E-mail: bulanoven@chem.unn.com
<https://doi.org/10.2298/JSC230722069B>



Particular attention should be paid to the problem of environmental pollution with lead, and its negative impact on the human body and animals. According to the provisions of the World Health Organization (WHO), lead is one of the 10 chemicals that cause the main concern from the point of view of public health and require action from Member States to protect workers, and children and women of childbearing age.

It should be noted that young children are particularly vulnerable to poisoning since 4–5 times more lead diffuses into their body compared to an adult organism.^{2,3} Quite often, the symptoms of poisoning do not appear, and this makes lead exposure an underestimated threat to the most common neurocognitive disorders. Until 2012, the “dangerous blood lead level” for children of more than 10 mg/dL. However, in May 2012, the Advisory Committee on Childhood Lead Poisoning Prevention (ACIP) recommended a value of 5 mg/dL.⁴ There is no “safe” concentration of lead in the blood; even such a low lead content in the blood can cause children to have a decrease in intelligence, behavioural disorders and learning difficulties.

The greatest impact on the environment is observed near local sources of pollution (for example, landfills of solid household waste, ore processing plants, metallurgical enterprises, as well as discarded sinkers and lead shot used for fishing or hunting). Natural emissions are also important sources of environmental lead pollution - the diffusion of natural lead from the earth's crust and mantle due to rock weathering and volcanic activity; the continued use of lead-containing paints in some countries (India, Vietnam, Mexico); the production and disposal of lead-acid batteries; products such as solder, pigments, jewellery, stained glass, ammunition, lead cable sheaths, *etc.*⁵ Organic lead compounds, previously used as leaded gasoline anti-detonators for internal combustion engines (0.1–0.3 %) increase the octane number and save fuel consumption) are more toxic than inorganic forms of lead. Their use in 1922 became one of the most serious environmental threats. However, August 30, 2021 was a significant date, which means the end of the use of leaded gasoline in the world.⁶

But despite the elimination of the most prominent threat of lead pollution in 2021, this problem remains unresolved. Other sources of pollution (lead paints and pigments still used in some countries, toys, cosmetics, pipe corrosion, *etc.*) require great attention and urgent measures. For example, in the UK, phosphates are added to drinking water to minimize the incoming amount of lead from water pipes.⁷

One of the chain reactions of soil contamination with lead is the contamination of groundwater. Lead can also get into the water due to unauthorized landfills and corrosion of water pipes. To solve this problem, it is necessary to create permeable reaction barriers (PRB) or zones of destructible reaction treatment.⁸

Permeable reaction barriers are an actively developing technology in which a unique reactive material is installed directly on the migration path of the water stream, which makes it cost-effective. Groundwater flows through the barrier and reacts with the material *in situ*, resulting in toxic metals: Pb, Cd, Co, etc. They are delayed, and the water is neutralised. However, PRB materials are effective if they are permeable enough to saturate with groundwater; react with pollutants; retain reactivity and permeability for a long time, and are cost-effective.^{9–11}

Apatite IITM – biogenic hydroxyapatite ($\text{Ca}_{10-x}\text{Na}_x(\text{PO}_4)_{6-x}(\text{CO}_3)_x(\text{OH})_2$, $x < 1$) obtained from dried fish bones has been recommended as an alternative material for the removal of Zn(II), Pb (II), Mn (II) and Fe (II) from groundwater. Column tests were carried out in which apatite reacted with ground water with an increase in pH to 6.5–7.0 and the release of metal phosphates. Metals precipitated in the form of $\text{Pb}_5(\text{PO}_4)_3\text{OH}$, $\text{Zn}_3(\text{PO}_4)_2 \cdot 4\text{H}_2\text{O}$, $\text{Mn}_3(\text{PO}_4)_2 \cdot 4\text{H}_2\text{O}$, $\text{Fe}_3(\text{PO}_4)_2 \cdot 8\text{H}_2\text{O}$, while the activity of apatite increased with a decrease in the acidity of water. Thus, the concentration of metals in ground water dropped from 30–75 to 0.10 mg/L.^{4,12,13}

An alternative way of binding lead is to directly precipitate it from the dissolved form, followed by the formation of compact ceramic materials for disposal.

However, both approaches raise questions about further work with the material: what to do with the substances, whether they are stable when ceramics are obtained from them, how stable the material is to temperature fluctuations in geological formations. It is assumed that the ceramics obtained from the interaction products will be stable for a long time and have good thermochemical properties due to the ability of apatite to encapsulate lead ions in its structure.

This work is devoted to the production of new lead compounds based on the aforementioned crystal-chemical type of apatite, as well as a systematic analysis of the crystal structure and thermal deformations accompanying the process of the final formation of the lead-recycling ceramic material on the example of new substances and a number of previously obtained and studied "classical" apatites ($\text{Pb}_5(\text{PO}_4)_3\text{F}$, $\text{Pb}_5(\text{PO}_4)_3\text{Cl}$, $\text{Pb}_5(\text{PO}_4)_3\text{I}$, $\text{Pb}_5(\text{VO}_4)_3\text{F}$, $\text{Pb}_5(\text{VO}_4)_3\text{Cl}$)^{14,15} and solid solutions based on them in $\text{Ca}_5(\text{PO}_4)_3\text{Cl}-\text{Pb}_5(\text{PO}_4)_3\text{Cl}$ ¹⁶ and $\text{Ca}_4\text{Bi}(\text{PO}_4)_3\text{O}-\text{Pb}_4\text{Bi}(\text{PO}_4)_3\text{O}$ systems.¹⁷

These compositions may be products of the interaction of the reaction material, apatite, with lead ions in ground water. Understanding the effect of the immobilization of lead in the structure of apatite on the solubility, crystallinity, surface activity and thermal stability of the reaction material is an urgent task.

EXPERIMENTAL

Sample preparation

In this paper, a number of compounds of the general composition $\text{Pb}_5(\text{A}^{\text{IV}}\text{O}_4)_2(\text{B}^{\text{VI}}\text{O}_4)$, $\text{Pb}_5(\text{A}^{\text{IV}}\text{O}_4)(\text{C}^{\text{V}}\text{O}_4)_2$ ($\text{A}^{\text{IV}} = \text{Si, Ge}$; $\text{B}^{\text{VI}} = \text{S, Cr}$; $\text{C}^{\text{V}} = \text{P}$) were considered.

These objects were chosen from the point of view of the high molar fraction of lead in the final compound, the absence of halogens that cause the binding of lead into phases of different composition, as well as from the point of view of the possibility of forming the crystal structure of apatite with a given chemical composition.

The synthesis was carried out by a solid-phase reaction using lead(II) nitrate $\text{Pb}(\text{NO}_3)_2$, silicon dioxide SiO_2 , pre-calcined to 873 K, germanium dioxide GeO_2 , diammonium hydrogen phosphate $(\text{NH}_4)_2\text{HPO}_4$, ammonium sulfate $(\text{NH}_4)_2\text{SO}_4$ and chromium trioxide (VI) CrO_3 . All compounds were produced by "Khimreactive" (Russian Federation) and have *puriss. spec.* quality.

The stoichiometric mixture of reagents was calcined in an alundum crucible, observing the stepwise process: 150–300 °C (decomposition of lead nitrate and ammonium salts), 300–600 °C (conversion of silicon oxide into a more reactive polymorphic modification,¹⁸ further, the heating was carried out in increments of 50 °C for 6 h until the monophase of the sample or the melting of the charge was reached. Dispersion was carried out every 2 h in an agate mortar using ethyl alcohol to create the additional wedging pressure and obtain a more finely dispersed product.

Sample characterization

The chemical purity and composition of the obtained samples were studied with Shimadzu XRF-1800 spectrometer using the fundamental parameters (FP) method with one standard sample. $\text{K}\alpha$ lines intensities were measured three times at 40 kV, 50 mA on Rh anode.

Powder diffractograms were taken using a Shimadzu XRD-6000 X-ray diffractometer: Cu $\text{K}\alpha$ radiation ($\lambda = 1.5406 \text{ \AA}$), Bregg–Brentano focusing, reflection shooting geometry, 2θ 10–60°, 0.02° step, scanning speed 2°/min.

Refinement of the crystal structure of compounds obtained for the first time ($\text{Pb}_5(\text{SiO}_4)(\text{PO}_4)_2$, $\text{Pb}_5(\text{GeO}_4)(\text{PO}_4)_2$) was carried out using the Rietveld method on the same diffractometer in the 2θ angle range 10–110°(120°), with 12 s signal dial time. Refinement of the crystal structure was carried out in the Topas 3.0 program.¹⁹ The background was described by a Chebyshev polynomial of the fourth degree. The peak profile was described by the pseudo-Voigt PV_TCHZ function. The crystal structure from the research²⁰ (ICSD #65240) was used as a model.

Visualization of a fragment of the crystal structure according to the data of full-profile refinement of powder XRD patterns was carried out in the Atoms v. 6.1.2 program.²¹

High-temperature X-ray diffraction experiments in the range from 298 to 873 K were carried out on the same diffractometer with increments of 0.02° ranging from 10 to 60° using an HA-1001 Shimadzu attachment. To calculate the thermal expansion coefficients and plot the thermal expansion diagram TTT 2.0 software were used.²²

The behaviour of individual compounds and composites in a wide range of temperature was investigated with thermoanalyser Shimadzu DTG-60H (heating rate 10 K/min, nitrogen atmosphere, alundum crucible).

The IR spectra of compounds were taken using a Shimadzu FTIR-8400s IR spectrometer to clarify the group structure and distortion of tetrahedral groups. The sample was prepared in the form of tablets $d = 15 \text{ mm}$ from a mixture with KBr ($\omega(\text{substance}) = 4 \%$), the interval of wave numbers was 4000–400 cm^{-1} , the number of scans was 30.

RESULTS AND DISCUSSION

Based on the data of powder XRD (Fig. 1) and X-ray fluorescence analysis (Table S-I of the Supplementary material to this paper), it was established that

only compounds whose stoichiometry corresponds to the compositions $\text{Pb}_5(\text{SiO}_4)(\text{PO}_4)_2$ ($\text{PbSiP}2$), $\text{Pb}_5(\text{GeO}_4)(\text{PO}_4)_2$ ($\text{PbGeP}2$), $\text{Pb}_5(\text{GeO}_4)_2(\text{CrO}_4)$ (PbGe2Cr) and $\text{Pb}_5(\text{GeO}_4)_2(\text{SO}_4)$ (PbGe2S) were obtained, and phosphate derivatives were obtained and identified for the first time. In addition, the IR spectroscopy method shows the absence of various condensed tetrahedral groups, such as $\text{P}_2\text{O}_7^{4-}$ and $\text{S}_2\text{O}_6^{2-}$ (Table S-II, Supplementary material).²³

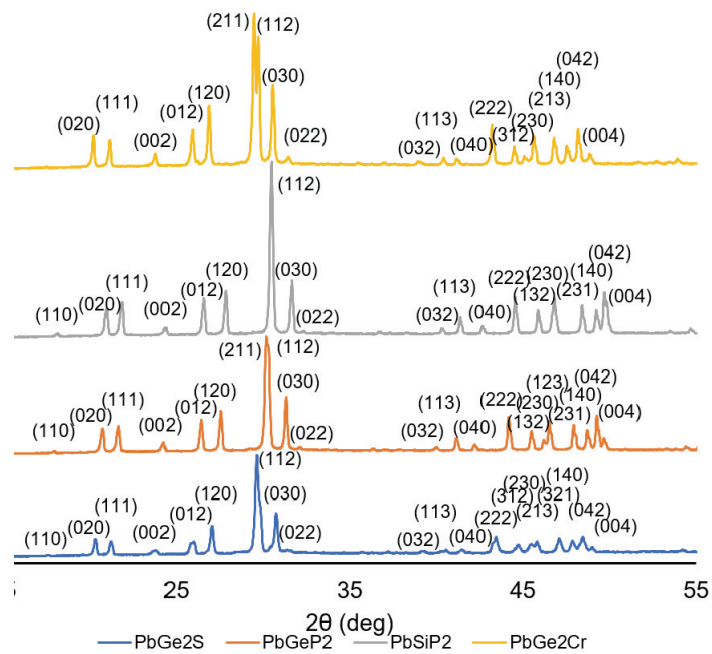


Fig. 1. XRD patterns of compounds under study

Results of the refinement of crystal structures of $\text{Pb}_5(\text{SiO}_4)(\text{PO}_4)_2$ and $\text{Pb}_5(\text{GeO}_4)(\text{PO}_4)_2$ are presented in Figs. 2 and 3 and in Tables I–III. Both compounds crystallise in the hexagonal syngony of the space group $P6_3/m$ and may be described in the framework of the classical crystal-chemical model of compounds with the structure of apatite.²⁴

The crystal structure of such compounds is constructed from quasi-layers formed by tetrahedral groups and lead cations at position 6*h*. The layers, in turn, are connected by the polyhedra of lead at position 4*f* (Fig. 3).

The structure of tetrahedral groups is strongly distorted if compared to an ideal tetrahedron: an undistorted tetrahedron has 9 oscillations in the IR range, however, due to the energy degeneracy in its spectrum, only 4 will be observed. The real spectra of the compounds under study are saturated with oscillation bands of various tetrahedral groups (Fig. 4, Table S-II), which indicates not only

the “standard” causes of spectrum complications (difference bands, composite bands, overtones, Fermi resonance) but also a strong distortion of tetrahedra.

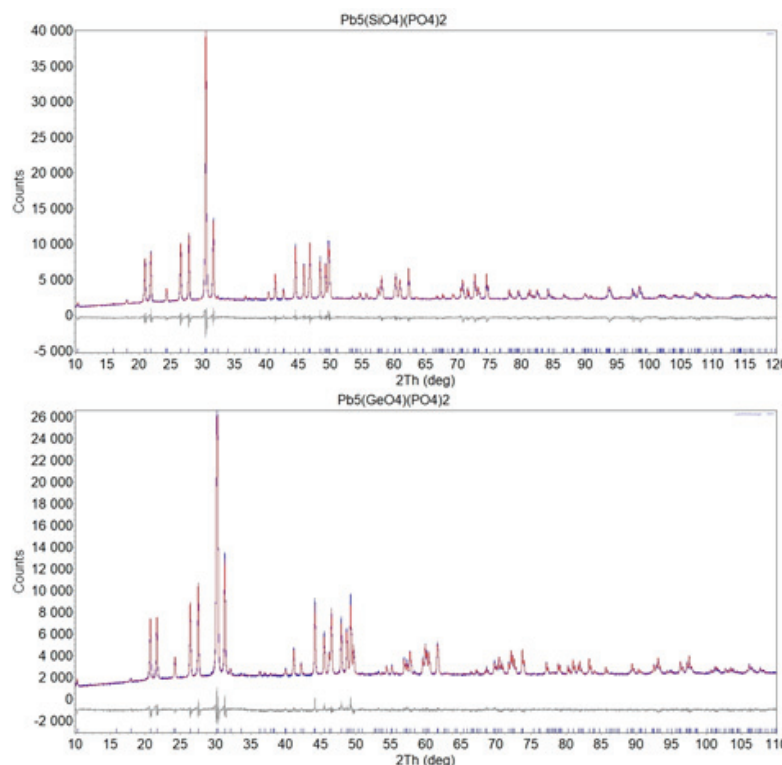


Fig. 2. Experimental, calculated, difference and stroke X-ray diffraction patterns of the new compounds.

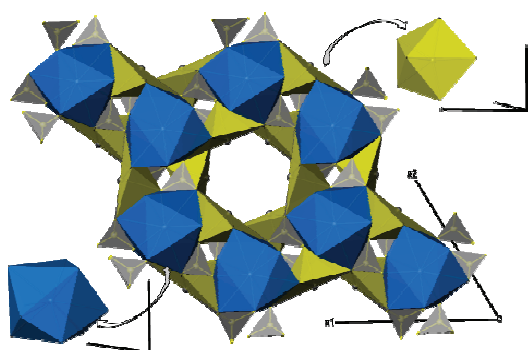


Fig. 3. Fragment of $\text{Pb}_5(\text{SiO}_4)(\text{PO}_4)_2$ crystal structure in projection along c -axis. Pb^{4h}O_9 polyhedron is shown in bottom left corner, Pb^{6h}O_6 polyhedron is in top right corner, $(\text{Si}/\text{P})\text{O}_4$ tetrahedra are also shown.

Calculation of bond lengths and valence angles based on crystallographic data (Table II) also demonstrate a strong distortion of tetrahedral groups, but in this case, the main reason will be the statistical substitution in the centre of the

tetrahedron of various elements (Si, Ge, P, Cr, S), very different in size (0.26, 0.39, 0.17, 0.345 and 0.12 Å, respectively).²⁵

TABLE I. Parameters and results of full-profile X-ray analysis of the crystal structures of the first-time-synthesized compounds

Parameter	Pb ₅ (SiO ₄)(PO ₄) ₂	Pb ₅ (GeO ₄)(PO ₄) ₂
Space group		P6 ₃ /m
<i>a</i> / Å	9.78782(16)	9.87697(12)
<i>c</i> / Å	7.31084(16)	7.33136(11)
<i>V</i> / Å ³	606.555(23)	619.388(17)
<i>M</i> / g·mol ⁻¹	2636.066	2725.107
Crystal size, nm	148.3(73)	130.0(38)
Density, g·cm ⁻³	7.21665(28)	7.30584(21)
Coefficients of pseudo-Voight function		
<i>U</i>	0.1986(66)	-0.0583(23)
<i>V</i>	-0.2103(65)	0.0789(29)
<i>Q</i>	0.0508(15)	-0.02398(88)
<i>Z</i>	0	0
<i>X</i>	0.0001(60)	0.0001(31)
<i>Y</i>	0	0
Scale factor	0.00008708(38)	0.00007836(30)
<i>R</i> -Bragg, %	4.694	1.730
<i>R</i> _{exp} / %	1.94/6.55	1.95/6.76
<i>R</i> _{wp} / %	4.66/15.71	3.83/13.27
<i>R</i> _p / %	3.35/18.89	2.78/16.08
<i>GOF</i>	2.40	1.96
<i>DW</i>	0.49	0.64

TABLE II. Atomic coordinates and occupancies of positions of new synthesized apatites

Atom	Wycoff position	<i>x</i>	<i>y</i>	<i>z</i>	<i>Occ</i>	<i>B</i> _{eq} / Å ²
Pb ₅ (SiO ₄)(PO ₄) ₂						
Pb1	4f	1/3	2/3	0.9987(18)	1	0.461(31)
Pb2	6h	0.24952(50)	0.99860(89)	1/4	1	0.461(31)
P	6h	0.3805(25)	0.3950(21)	1/4	2/3	0.52(35)
Si					1/3	0.52(35)
O1	6h	0.4444(35)	0.3274(33)	1/4	1	0.46(38)
O2	6h	0.4778(30)	0.5619(29)	1/4	1	0.46(38)
O3	12i	0.2700(19)	0.3494(14)	0.0685(22)	1	0.46(38)
Pb ₅ (GeO ₄)(PO ₄) ₂						
Pb1	4f	1/3	2/3	0.9923(14)	1	0.538(28)
Pb2	6h	0.24943(37)	0.99694(63)	1/4	1	0.538(28)
P	6h	0.3824(17)	0.3906(15)	1/4	2/3	0.68(18)
Ge	6h				1/3	0.68(18)
O1	6h	0.4503(30)	0.3336(29)	1/4	1	1.16(36)
O2	6h	0.4946(24)	0.5730(24)	1/4	1	1.16(36)
O3	12i	0.2593(16)	0.3432(13)	0.0715(18)	1	1.16(36)

TABLE III. Parameters of the Pb^{4f}O_9 coordination polyhedron in the crystal structure of mixed-tetrahedral apatites under consideration

Distance and angle	$\text{Pb}_5(\text{SiO}_4)(\text{PO}_4)_2$	$\text{Pb}_5(\text{GeO}_4)(\text{PO}_4)_2$	$\text{Pb}_5(\text{GeO}_4)_2(\text{SO}_4)$	$\text{Pb}_5(\text{GeO}_4)_2(\text{CrO}_4)$
$\text{M}^{4f}\text{--O}_2 \times 3, \text{\AA}$	2.807(28)	2.882(22)	2.833	2.833
$\text{M}^{4f}\text{--O}_1 \times 3, \text{\AA}$	2.813(30)	2.802(25)	2.494	2.469
$\text{M}^{4f}\text{--O}_3 \times 3, \text{\AA}$	2.892(15)	2.950(13)	2.956	2.972
$\varphi / {}^\circ$	26.1	21.2	25.2	25.8

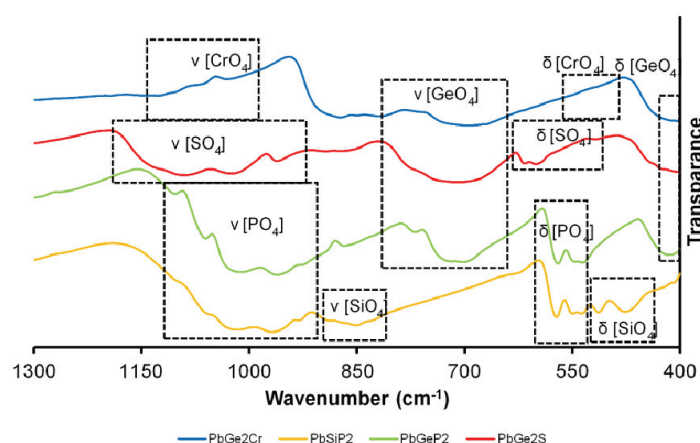


Fig. 4. IR spectra of synthesized mixed-tetrahedral apatites with line assignments.

The cations located in the crystallographic position $6h$, as a rule, form coordination polyhedra with CN 7–9: pentagonal bipyramids, two- and three-cap trigonal prisms. In this case, as can be seen from the example of a fragment of the structure (Fig. 3), it is a pentagonal pyramid in question. However, this type of structural element is due to the specifics of the visualization software. The electronic structure of lead atoms has a fundamental difference from the numerous cations capable of forming the structure of apatite: being a p-element, lead has a stereochemically active electron $6s$ pair, which is located in the formally missing vertex of the pentagonal bipyramid, and directly in the structure is deployed in the area of a hexagonal channel running along the crystallographic axis c .

The cations in the crystallographic position $4f$ are always three-cap trigonal prisms of varying degrees of distortion. The distortion of this structural element is estimated by the twist angle.²⁶ As can be seen from the data in Table III, in the compounds under consideration, they are in a fairly narrow range of values characteristic of the structural type as a whole.

For the analysis of thermal expansion, the temperature dependences of the parameters of elementary cells are constructed, which are then approximated by linear or quadratic functions, according to the coefficients of which those of ther-

mal expansion are calculated in the TTT 2.0 software. A similar operation for compounds with the structure of apatite was given step by step in our previous works,^{14,15} and here we would like to focus on specific results and conclusions.

First of all, it is worth noting that based on the results of the DSC (Fig. 5), it was decided to conduct high-temperature X-ray studies in the temperature range of 298–873 K, and the available data on other lead-containing apatites should be limited to a similar range (Fig. 6). It is also worth noting here that, unlike the vast majority of “classical” Pb-apatites, no anomalies were detected on the DSC curves of mixed-tetrahedral compounds and during the high-temperature X-ray experiment, suggesting the presence of polymorphic transformations.¹⁴

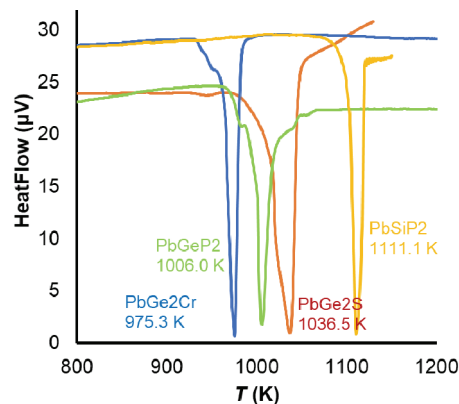


Fig. 5. DSC curves for synthesized mixed-tetrahedral apatites near melting points.

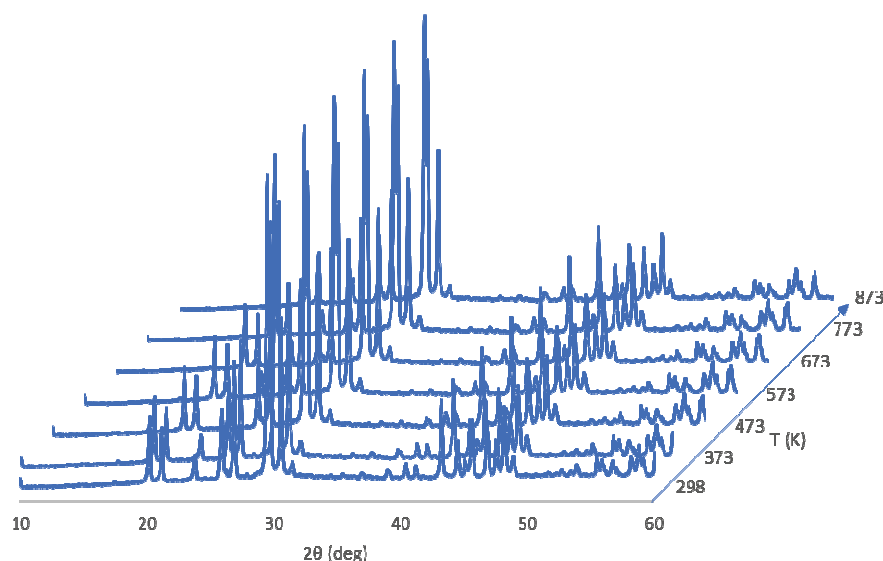


Fig. 6. HTXRD patterns of $\text{Pb}_5(\text{GeO}_4)_2(\text{CrO}_4)$.

Secondly, earlier we provided data on the values of the coefficients of thermal expansion exclusively along the crystallographic directions a and c and, thus, we obtained a characteristic of the crystal structure or of a single-crystal material. Of course, in the case of the hexagonal syngony under consideration, the main directions of the thermal expansion tensor and the crystallographic directions are strictly fixed relative to each other, and the values of the coefficients coincide. Therefore, for the completeness, Fig. 7 shows as an example a three-dimensional temperature surface of thermal expansion $\text{Pb}_5(\text{SiO}_4)(\text{PO}_4)_2$ at a temperature of 873 K, indicating the directions of the main directions of the tensor and the crystallographic axes. It is also worth noting that for the lead-containing apatites under consideration, the temperature dependencies of the linear coefficients of thermal expansion are shown in Table S-III of the Supplementary material, but for a potential material representing a ceramic polycrystalline sample, these data cannot be directly transferred due to the statistical orientation of microcrystals in space. However, the volumetric coefficient of thermal expansion (Table IV), as an integral quantity characterizing the behaviour of the material, can be used for analysis.

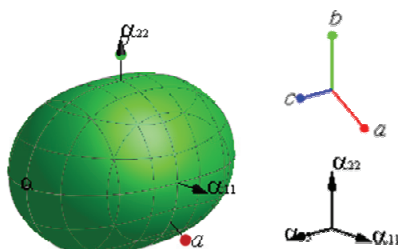


Fig. 7. Thermal expansion diagram $\text{Pb}_5(\text{SiO}_4)(\text{PO}_4)_2$ at 873 K, indicating the directions of the crystallographic axes and the main components of the thermal deformation tensor.

In the case of individual compounds with the apatite structure, it is seen that the nature of temperature dependencies (the rate of change is $0.02\text{--}0.03 \times 10^6 \text{ K}^{-1}$ per K) and the values of thermal expansion ($40\text{--}70 \times 10^6 \text{ K}^{-1}$) converge, which confirms the previously stated assumption about the fundamental influence of metal cations in the composition of apatites on the nature of thermal deformations.¹⁵ The abnormal behaviour of (rate of change $\sim 0.1 \times 10^6 \text{ K}^{-1}$ per K; interval $1\text{--}66 \times 10^6 \text{ K}^{-1}$) $\text{Pb}_5(\text{PO}_4)_I$ compound is most likely due to the high defect of the structure, which was shown in a recent paper. The $\text{Pb}_5(\text{PO}_4)_3\text{F}$ compound also arouses similar suspicions (the rate of change is $\sim 0.06 \times 10^6 \text{ K}^{-1}$ per K; the interval is $30\text{--}67 \times 10^6 \text{ K}^{-1}$). The remaining “classical” and mixed-tetrahedral apatites behave without any anomalies.

Volumetric coefficients of thermal expansion of solid solutions of systems $(\text{Ca}_x\text{Pb}_{1-x})_5(\text{PO}_4)_3\text{Cl}$ and $(\text{Ca}_x\text{Pb}_{1-x})_4\text{Bi}_2(\text{PO}_4)_6\text{O}$ lie in a rather narrow range of values ($30\text{--}60 \times 10^6 \text{ K}^{-1}$), and lower than in the case of individual substances, with the exception of the composition $\text{Ca}_{2.5}\text{Pb}_{2.5}(\text{PO}_4)_3\text{Cl}$, which differs both in

the anomalous values of the coefficient (interval $16\text{--}106 \times 10^6 \text{ K}^{-1}$) and the angle of inclination of its temperature dependencies (the rate of change is $\sim 0.16 \times 10^6 \text{ K}^{-1}$ per K). The only assumption about the reason for this effect is the formation of an internal ordering of the distribution of calcium and lead ions in the positions of the crystal structure, instead of the statistical distribution inherent in solid solutions.

TABLE IV. Temperature dependencies of volume (α_V) thermal expansion coefficients for “classical” apatites (column 1–5), mixed-tetrahedral apatites (column 6–9), solid solutions in $(\text{Ca}_x\text{Pb}_{1-x})_5(\text{PO}_4)_3\text{Cl}$ (column 10–12) and $(\text{Ca}_x\text{Pb}_{1-x})_4\text{Bi}_2(\text{PO}_4)_6\text{O}$ (column 13–15) systems; Standard uncertainties, $u = 0.02 \text{ wt. \%}$

T / K	1	2	3	4	5
	PbPF	PbPCl	PbPI	PbVF	PbVCl
298	30.0	39.1	1.0	40.5	46.5
373	34.8	41.6	9.6	42.5	48.1
473	41.2	45.0	20.9	45.2	50.2
573	47.6	48.3	32.3	47.8	52.2
673	53.9	51.6	43.6	50.5	54.3
773	60.2	54.9	54.8	53.1	56.3
873	66.5	58.1	66.0	55.7	58.4
T / K	6	7	8	9	10
	PbSiP2	PbGeP2	PbGe2S	PbGe2Cr	Ca3.5Pb1.5
298	46.4	43.8	49.0	54.1	35.6
373	48.6	45.9	51.9	56.3	38.3
473	51.5	48.6	55.8	59.1	41.9
573	54.4	51.4	59.6	61.9	45.5
673	57.3	54.1	63.5	64.7	49.0
773	60.2	56.8	67.3	67.5	52.6
873	63.0	59.5	71.0	70.2	56.1
T / K	11	12	13	14	15
	Ca2.5Pb2.5	Ca1.25Pb3.75	Ca6Pb2Bi2	Ca4Pb4Bi2	Ca2Pb6Bi2
298	16.1	34.5	32.1	35.0	38.0
373	28.0	37.0	34.6	37.9	40.7
473	43.8	40.3	37.9	42.2	44.2
573	59.5	43.6	41.2	46.6	47.7
673	75.2	46.8	44.4	50.9	51.2
773	90.7	50.0	47.7	55.2	54.7
873	106.1	53.2	50.9	59.5	58.1

From the point of view of binding lead for a long time into a ceramic matrix, its solid solutions with calcium look promising. Their advantages include lower values of thermal expansion coefficients, low rates of thermal deformation, and high melting temperatures. In addition, such a composition of the binding matrix has proven itself in the development of immobilizers of the Apatite IITM type.^{4,12,13} However, from the point of view of further compaction and binding,

there remains a high risk associated with the restructuring of the structure and the accompanying change in thermal deformations, as well as abnormal orderings in the crystal structure.

“Classical” apatites also raise concerns in terms of polymorphism. An additional limiting factor is the presence of halogen in their composition. A number of studies have demonstrated a low stability of halogen retention in the apatite matrix in leaching experiments,^{27,28} which may lead to an increase in the defectiveness of the material up to its destruction.

Thus, among the remaining mixed tetrahedral compounds for further study, the most promising is the composition $\text{Pb}_5(\text{SiO}_4)(\text{PO}_4)_2$, which, in addition to relative thermal stability and the lowest level of thermal deformations among the analogues under consideration, has the advantage of simplicity and accessibility of the chemical composition.

CONCLUSION

This paper presents the results of the search for new phases to solve an urgent environmental problem – lead binding for long-term isolation from the environment, as well as an assessment of their prospects in terms of crystal chemical (composition, structure) and thermophysical (melting point, thermal expansion) data.

In the course of work it was not only possible to obtain two new mixed-tetrahedral compounds with apatite structure $(\text{Pb}_5(\text{SiO}_4)(\text{PO}_4)_2$ ($a = 9.78782(16)$ Å, $c = 7.31084(16)$ Å, $V = 606.555(23)$ Å³, $R_{\text{bragg}} = 4.694$ %) and $\text{Pb}_5(\text{GeO}_4)(\text{PO}_4)_2$ ($a = 9.87697(12)$ Å, $c = 7.33136(11)$ Å, $V = 619.388(17)$ Å³, $R_{\text{bragg}} = 1.730$ %) and characterize them in terms of crystal structure and thermal deformations, but also on the basis of thermal expansion analysis from the sample of lead-containing apatites extended due to earlier studies, to find a subclass characterised by low values of thermophysical parameters indicators (the rate of change of linear thermal expansion coefficients is $0.02\text{--}0.03 \times 10^6$ K⁻¹; values of the volume thermal expansion coefficients are $40\text{--}70 \times 10^6$ K⁻¹), which gives grounds to consider it as a potential chemical basis for the creation of materials for the lead immobilization for lead.

Of course, the above conclusions are not exhaustive and should be subsequently supplemented by a study of lead leaching rates from the proposed matrix under conditions as close as possible to real operating conditions. However, a non-trivial approach allowed us to detect a number of new compounds $\text{Pb}_5(\text{SiO}_4)(\text{PO}_4)_2$, $\text{Pb}_5(\text{GeO}_4)(\text{PO}_4)_2$ along with previously known $\text{Pb}_5(\text{GeO}_4)_2(\text{CrO}_4)$ and $\text{Pb}_5(\text{GeO}_4)_2(\text{SO}_4)$, but were out of sight, the use of which can solve the lead pollution problem faster.

SUPPLEMENTARY MATERIAL

Additional data and information are available electronically at the pages of journal website: <https://www.shd-pub.org.rs/index.php/JSCS/article/view/12511>, or from the corresponding author on request.

Acknowledgements. The authors are grateful to V.Zh. Korokin, Ph.D., for some of the syntheses carried out. The research was carried out with financial support *via* State assignment in Research scientific laboratory of “Chemistry of natural products and their synthetic analogues” of Scientific Educational Centre “Technoplatform 2035” (project FSWR-2021-014).

ИЗВОД

ПРОНАЛАЖЕЊЕ НОВИХ АПАТИТНИХ ФАЗА ЗА ИСКОРИШЋЕЊЕ ОЛОВА НА
ОСНОВУ КРИСТАЛНЕ СТРУКТУРЕ И ТОПЛОТНОГ ШИРЕЊА

EVGENY N. BULANOV, ANASTASYYA A. VASILEVA, OXANA N. GOLITSYNA, ALYONA G. SHVAREVA
и ALEXANDER V. KNYAZEV

Lobachevsky University, 23 Gagarin ave, Nizhny Novgorod 603022, Russia

Апатити, као једна од најзначајнијих група минералних структура, се разматрају као матрица за имобилизацију јона олова, који имају негативан утицај на биосферу. Кристално-хемијски (состав, структура) и термофизички аспект (топлотно ширење) се узимају као основа за анализу особина ове класе материјала. Сугерише се да су супстанце састава $Pb_5(A^{IV}O_4)_2(B^{VI}O_4)$ и $Pb_5(A^{IV}O_4)(C^V O_4)_2$ апатитне структуре одговарајућа форма за имобилизацију олова, при чему је $A^{IV} = Si, Ge; B^{VI} = S, Cr$ и $C^V = P$. Ове компоненте, као што је показано помоћу диференцијално-термијске анализе (DTA) и високо-температурне рендгенске анализе (HTXRD), одликују се одсуством полиморфизма и абнормалног уређења структуре. Такође, имају релативно мале вредности термофизичких индикатора (брзина промене линеарног коефицијента топлотног ширења је $0.02 - 0.03 \times 10^{-6} \text{ K}^{-1}$, вредности запреминског коефицијента ширења су $40 - 70 \times 10^{-6} \text{ K}^{-1}$). По први пут су добијене, идентификоване и кристалографски окарактерисане компоненте $Pb_5(SiO_4)(PO_4)_2$ ($a = 9,78782(16) \text{ \AA}$, $c = 7,31084(16) \text{ \AA}$, $V = 606,555(23) \text{ \AA}^3$, $R\text{-bragg} = 4,694\%$) и $Pb_5(GeO_4)(PO_4)_2$ ($a = 9,87697(12) \text{ \AA}$, $c = 7,33136(11) \text{ \AA}$, $V = 619,388(17) \text{ \AA}^3$, $R\text{-bragg} = 1,730\%$).

(Примљено 24. јула, ревидирано 31. јула, прихваћено 18. септембра 2023)

REFERENCES

- Food and Agriculture Organization of the United Nations, *Polluting our soils is polluting our future*, <https://www.fao.org/fao-stories/article/en/c/1126974/> (accessed: July 22, 2023)
- World Health Organization, *Lead poisoning*, <https://www.who.int/news-room/fact-sheets/detail/lead-poisoning-and-health> (accessed: July 22, 2023)
- L. Chandran, R. Cataldo, *Pediatr. Rev.* **31** (2010) 399 (<https://doi.org/10.1542/pir.31-10-399>)
- W. A. Martin, S. L. Larson, D. R. Felt, J. Wright, C. S. Griggs, M. Thompson, J. L. Conca, C. C. Nestler, *Appl. Geochem.* **23** (2008) 34 (<https://doi.org/10.1016/j.apgeochem.2007.08.005>)
- United Nations Environment Programme, *Key scientific findings for lead: an excerpt from Final review of scientific information on lead*, https://wedocs.unep.org/bitstream/handle/20.500.11822/22871/Key_Scientific_Findings_Lead_RU.pdf?sequence=5&isAllowed=y (accessed: July 22, 2023)

6. United Nations Environment Programme, *Era of leaded petrol over, eliminating a major threat to human and planetary health*, <https://www.unep.org/news-and-stories/press-release/era-leaded-petrol-over-eliminating-major-threat-human-and-planetary> (accessed: July 22, 2023)
7. J. D. Hopwood, G. R. Derrick, D. R. Brown, C. D. Newman, J. Haley, R. Kershaw, M. Collinge, *J. Chem.* **2016** (2016) 9074062 (<https://doi.org/10.1155/2016/9074062>)
8. I. S. Kasimov, A. E. Vorob'ev, *Geochemical barriers in the hypergenesis zone*, MSU Publishing House, Moscow, 2002
9. J. Oliva, J. De Pablo, J. L. Cortina, J. Cama, & C. Ayora, *J. Hazard. Mater.* **194** (2011) 312 (<https://doi.org/10.1016/j.jhazmat.2011.07.104>)
10. M. Katoh, A. Makimura, T. Sato, *Environ. Technol. (UK)* **37** (2016) 3036 (<https://doi.org/10.1080/09593330.2016.1174744>)
11. S. Bailliez, A. Nzihou, E. Bèche, G. Flamant, *Process Saf. Environ. Prot.* **82** (2004) 175 (<https://doi.org/10.1205/095758204322972816>)
12. J. Oliva, J. De Pablo, J. L. Cortina, J. Cama, C. Ayora, *J. Hazard. Mater.* **184** (2010) 364 (<https://doi.org/10.1016/j.jhazmat.2010.08.045>)
13. J. Oliva, J. Cama, J. L. Cortina, C. Ayora, J. De Pablo, *J. Hazard. Mater.* **213–214** (2012) 7 (<https://doi.org/10.1016/j.jhazmat.2012.01.027>)
14. N. G. Chernorukov, A. V. Knyazev, E. N. Bulanov, *Inorg. Mater.* **47** (2011) 172 (<https://doi.org/10.1134/S002016851101002X>)
15. A. V. Knyazev, N. G. Chernorukov, E. N. Bulanov, *Mater. Chem. Phys.* **132** (2012) 773 (<https://doi.org/10.1016/j.matchemphys.2011.12.011>)
16. A. V. Knyazev, E. N. Bulanov, V. Z. Korokin, *Mater. Res. Bull.* **61** (2014) 47 (<https://doi.org/10.1016/j.materresbull.2014.09.089>)
17. E. N. Bulanov, K. S. Stasenko, O. N. Golitsyna, V. M. Kyashkin, A. V. Knyazev, *Ceram. Int.* **48** (2022) 9858 (<https://doi.org/10.1016/j.ceramint.2021.12.188>)
18. M. Mosesman, K. Pitzer, *J. Am. Chem. Soc.* **63** (1941) 2348 (<https://doi.org/10.1021/ja01854a013>)
19. A. A. Coelho, *J. Appl. Crystallogr.* **51** (2018) 210 (<https://doi.org/10.1107/S1600576718000183>)
20. G. Engel, B. Deppisch, *Z. anorg. allg. Chem.* **562** (1988) 131 (<https://doi.org/10.1002/zaac.19885620116>)
21. Atoms, V. 6.1.2, by Shape Software, 2006
22. R. S. Bubnova, V. A. Firsova, S. K. Filatov, *Glas. Phys. Chem.* **39** (2013) 347 (<https://doi.org/10.1134/S108765961303005X>)
23. K. Nakamoto, *Infrared and Raman Spectra of Inorganic and Coordination Compounds*, Fourth Edi John Wiley and Sons, Inc., New York, 1986
24. T. White, C. Ferraris, J. Kim, S. Madhavi, *Apatite - an adaptive framework structure*, 2018 (<https://doi.org/10.2138/rmg.2005.57.10>)
25. R. D. Shannon, *Acta Crystallogr., A* **32** (1976) 751767 (<https://doi.org/10.1107/S0567739476001551>)
26. S. C. Lim, T. Baikie, S. S. Pramana, R. Smith, T. J. White, *J. Solid State Chem.* **184** (2011) 2978 (<https://doi.org/10.1016/j.jssc.2011.08.031>)
27. M. Zhang, E. R. Maddrell, P. K. Abraitis, E. K. H. Salje, *Mater. Sci. Eng., B* **137** (2007) 149 (<https://doi.org/10.1016/j.mseb.2006.11.003>)
28. Z. Zhang, A. Heath, K. T. Valsaraj, W. L. Ebert, T. Yao, J. Lian, J. Wang, *RSC Adv.* **8** (2018) 3951 (<https://doi.org/10.1039/c7ra11049a>).